A complete thermo–electro–viscoelastic characterization of dielectric elastomers, Part I: Experimental investigations

Markus Mehnert [a,*], Mokarram Hossain [c], Paul Steinmann [a,b]

[a] *Institute of Applied Mechanics, University of Erlangen–Nuremberg, Egerlandstr. 5, 91058 Erlangen, Germany*
[b] *Glasgow Computational Engineering Centre (GCEC), University of Glasgow, United Kingdom*
[c] *Zienkiewicz Centre for Computational Engineering, College of Engineering, Bay Campus, Swansea University, Swansea, United Kingdom*

ARTICLE INFO

ABSTRACT

Dielectric elastomers are a class of solid polymeric materials that are sufficiently soft to deform under the application of an electric field due to the interaction of quasi-static electric charges. Their potential to undergo large deformations renders them promising candidates for the design of energy harvesters, sensors and soft actuators. For their application however, the influence of additional thermal effects should be taken into account as the base materials frequently show a distinct thermal sensitivity that drastically influences their mechanical response. This contribution presents the results of a wide range of experiments conducted on the popular dielectric elastomer VHB 4905™ under a combination of mechanical, thermal and electric loading scenarios. These experiments are performed in such a way that the obtained results are well suited for the identification of the necessary material parameters appearing in a thermo–electro–viscoelastic constitutive model that will subsequently be presented in the second part of the contribution.

1. Introduction

Over the last two decades, there has been an ever-expanding demand for technology that combines multi-functionality, robustness and miniature dimensions with low production costs. Such a motivation lead to an increased interest in multi-functional smart materials, which possess the ability to react to non-mechanical stimuli with a change of their shape or mechanical properties. These characteristics can be found in electro-active polymers (EAPs), which is a collective term used for polymeric materials that have the potential to undergo large deformations and changes in their material properties due to the application of an electric field. EAPs may outperform traditional technologies such as shape memory alloys or electroactive ceramics in the design of actuators especially when low weight and small production costs paired with a reasonable reaction time are the dominating requirements (Pelrine et al., 2000a,b). The properties of EAPs open up revolutionary design possibilities for example in the field of soft robotics, where flexible grippers can be used for the handling of sensitive objects and decrease the risk of accidents in the interaction between machine and user. Furthermore, a wide range of other applications like sensors, generators or adaptable optics have demonstrated the extraordinary potential of electro-active polymers (O'Halloran et al., 2008; Bar-Cohen, 2002, 2004; Vertechy et al., 2014; Böse and Fuß, 2014; Koh et al., 2011a). Dielectric elastomers (DE) are a popular subclass of EAPs, due to their comparably simple handling and commercial availability. The simplest form of a soft actuator produced from EAPs consists of two compliant electrodes in form of an electrically conductive layer, applied to both sides of a thin film of a dielectric elastomer (Carpi et al., 2015). Upon
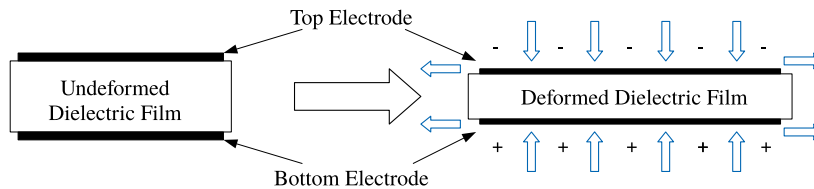
Fig. 1. Working principle of a soft actuator consisting of a dielectric thin film sandwiched between a pair of compliant electrodes. Application of an electric potential difference results in a deformation of the dielectric material.

the application of a voltage difference, the Coulomb forces between the charged electrodes lead to a contraction of the thin film in the direction of the electric field as depicted in the sketch in Fig. 1.

While the material contracts in the thickness direction as a result of the applied electric voltage, it expands in the lateral direction due to the positive Poisson ratio of the underlying rubber-like material and the repelling forces between the similar charges on the capacitor (Bustamante, 2009; Dorfmann and Ogden, 2005). The applied coating can deform with the thin film sandwiched in between without significantly influencing the material response, hence it is called 'compliant'. The magnitude of the resulting deformation is limited primarily by the occurrence of electromechanical instabilities (EMI) such as pull-in instabilities, which is caused by a positive feedback between the increase of the electric field and the thinning of the material (Wang et al., 2016; Sheng et al., 2013). This unstable material response can potentially be suppressed by precautions such as the application of pre-stretch (Koh et al., 2011b), nonlinear polarization (Li et al., 2011) or the incorporation of an interpenetrating network (Ha et al., 2006).

Note that most of the polymeric materials used as EAPs are moderate to highly sensitive to temperature changes (Ferry, 1980; Lion, 2000; Guo et al., 2015). These thermal effects are visible on the one hand through thermal expansion that leads to significant volumetric deformations of the material depending on the thermal expansion coefficient (Lion, 1997b). On the other hand, the mechanical properties typically show a significant sensitivity to thermal loading. According to Treloar (1975), the dependency of the elastic response shows a linear correlation with the temperature resulting in an increase in the stresses and consequently an increase in the material stiffness due to a temperature increase for rubbery materials. In the case of cyclic loading tests, on the other hand, it can be observed that the rate dependency decreases with an increase in temperature (Bhagawan and De, 1988; Lion, 1997a). These effects on the material properties naturally also influence the instability behavior of dielectric elastomers, as shown for example in the contributions by Sheng et al. (2011, 2012a, 2013), Guo et al. (2021) or Liu et al. (2011).

Currently, there is still a significant shortage of reliable experimental data to develop a clear understanding of the effects of thermo–electro–mechanically coupled loads on any electro-active polymers. Furthermore, the data that is available is frequently obtained from experiments performed under conditions that are not well suited for the identification of the material parameters appearing in a thermo–electro–mechanically coupled constitutive model at finite strain. For instance, in the case of DEs experiments conducted under an electro-mechanical load, the work of Diaconu et al. (2006) had been the only popular source of experimental data for years. However, these experiments were conducted at room temperature. This situation has changed only slightly in last few years with the publication of experimental works on some popular dielectric elastomers such as the commercially available VHB 4910™ by 3M™ or the silicone-based Ecoflex™ that has been gaining increasing attention recently in the EAP community. For VHB 4910™, a number of standard tests were performed by Hossain and co-workers demonstrating the material's highly viscoelastic nature. These essential experiments include single- and multi-step relaxation tests, cyclic loading–unloading tests at various strains and strain rates (Hossain et al., 2012). Afterwards, they used a micro-mechanically motivated viscoelastic framework and identified all relevant material parameters appearing in the constitutive model. Following the contribution, Hossain and co-workers further experimentally characterized the electro-mechanical behavior of the same material (Hossain et al., 2015). However, due to the prestretch that was applied manually in order to amplify the influence of the electric field, these results were not well suited for the identification of the electro-mechanical coupling parameters. Moreover, similar to Diaconu and co-workers (Diaconu et al., 2006), Hossain et al. (2015) performed their electro-mechanical tests discarding the influence of temperature. Very recently, comprehensive experimental studies were performed on VHB 4910™ by considering the effects of a wide range of temperatures on the material behavior, see for example, Liao et al. (2020) and Zhang et al. (2020). However, these tests were not conducted under an electric field.

Despite significant efforts in the experimental characterizations of dielectric elastomers under thermo–mechanical conditions, to the best of the authors' knowledge, a rigorous experimental study considering the thermo–electro–viscoelastic characteristics of any DEs is not available in the literature to date. Hence, this contribution is intended to fill up the gap by performing a comprehensive thermo–electro–mechanical characterizations of a classical polymer used as a DE. For that, a widely used acrylic-based dielectric elastomer VHB 4905™ is selected which not only demonstrates large actuations but also shows a significant time-dependent viscoelastic behavior with a high temperature sensitivity.

The work is organized as follows: in Section 2, the different testing setups are described in detail. The following Section 3 presents the results of the conducted experiments that are obtained only from purely mechanical tests, followed by the thermo–mechanical experiments. For the sake of completeness, the results of the electro-mechanical experiments that have already been published in Mehnert et al. (2019) are added in the subsequent Section 3.3. Finally, the data obtained in experiments with a combination of mechanical, thermal and electric loads are shown in 3.4. The paper is closed by few concluding remarks.
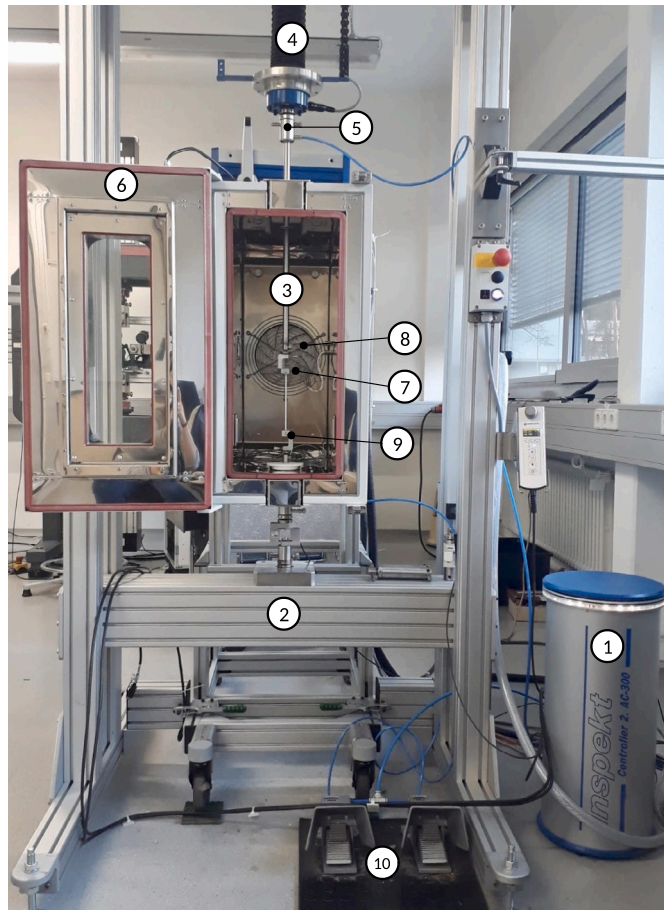
Fig. 2. Deformed state material sample mounted in the single-spindle testing machine Hegewald & Peschke *Inspekt S 5 kN*. *Legend:* **1** control unit, **2** aluminum test frame, **3** single-spindle load unit, **4** bellow seals, **5** force transducer, **6** temperature chamber, **7** integrated fan, **8** temperature sensors, **9** pneumatic clamps, **10** foot pedals.

2. Experimental setup

In order to complete all relevant experiments, different experimental setups were used. The mechanical and thermo–mechanical tests were performed on the single-spindle testing machine Hegewald & Peschke *Inspekt S 5 kN* in combination with the thermo chamber *T54 LN2* by Mytron depicted in Fig. 2. The device consists of a control unit (1) located in a separate case, a rigid aluminum test frame (2), a single-spindle load unit driven by an AC servomotor (3), bellow seals (4) that protect the single spindle against dirt or possible oil leakage, a force transducer (R-load cell 5 kN, Hegewald & Peschke) (5) and the temperature chamber (6) with an integrated fan (7) and temperature sensors (8). The machine is connected to the local compressed air supply system. Thus, the material sample can be mounted into the testing device using pneumatically activated clamps (9) controlled via foot pedals (10). The force transducer calculates the measured force with a standard deviation of $\pm$ 0.01% (calibration class 1 acc. to DIN EN ISO 7500), converts it into an electrical signal and sends it to the connected PC for data acquisition. The temperature can be increased from room temperature of 23 °C up to 180 °C by an inflow of pre-heated air. Due to the internal dimensions of the thermo chamber, the maximum displacement of the single-spindle is restricted to 350 mm at a traverse speed of up to 33 mm/s.

As the *Inspekt 5 kN* is not equipped for the application of high electric voltages on the material samples, the electro-mechanical and thermo–electro–mechanical experiments were performed on a custom-made testing device. However, initially this testing device did not include a thermo chamber for the regulation of the temperature. Therefore, after the initially performed electro-mechanical experiments on VHB 4905™ that were published in Mehnert et al. (2019), the testing device was significantly modified to include a temperature regulation. The initial setup prior to the modification, as depicted in Fig. 3, consists of seven major parts. The material sample (**1**) is mounted in the machine at both ends by a pair of clamps (**2**). The clamps on the bottom are attached to the movable table, which is actuated by a high precision linear translation stage (**3**). The top pair is fixed to the force transducer (**4**) (model number GSO-1 K, Transducer Techniques, USA) that in turn is connected to the frame of the testing system (**5**). In order to apply an electric field, both sides of the material sample are connected to a power source. This is achieved by an electric wiring (**6**) that can move freely during the deformation of the material and that is connected to a separate power supply. In order to ensure work
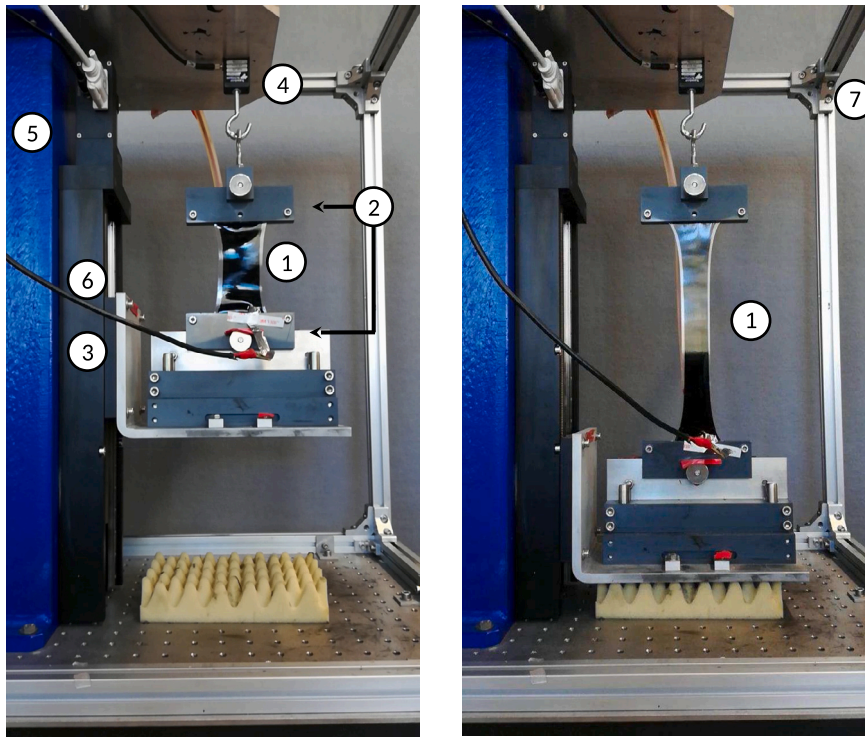
Fig. 3. Coated test sample of VHB 4905™ in the (left) undeformed and (right) deformed state. *Legend:* **1** coated test sample, **2** clamping plates, **3** linear stage with movable table, **4** force transducer, **5** frame, **6** electric wiring, **7** safety cabinet.
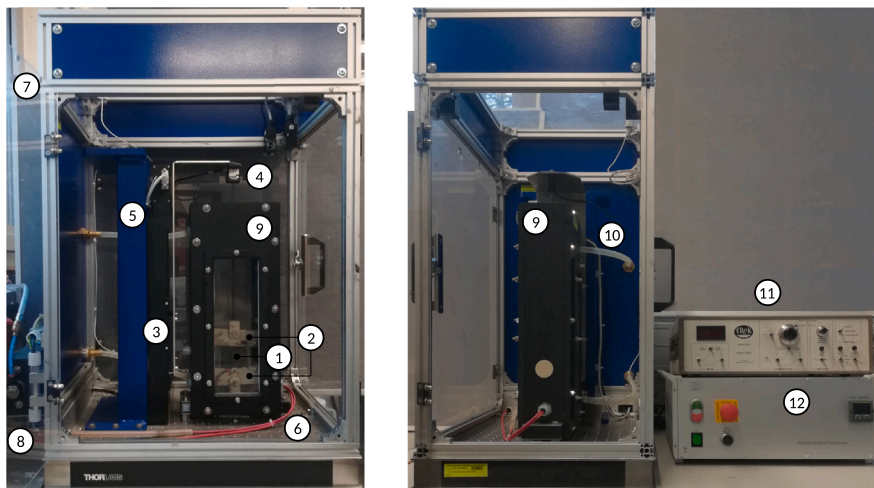

Fig. 4. Coated test sample of VHB 4905™ mounted inside the thermal chamber depicted in (left) side view and (right) front view. *Legend:* **1** coated test sample, **2** clamping plates, **3** linear stage, **4** force transducer, **5** frame, **6** electric wiring, **7** safety cabinet, **8** heating system, **9** thermo chamber, **10** ventilation tubes, **11** control unit, **12** power supply.

safety, a non-conductive cabinet (**7**) encloses the entire setup. During the experiments, samples are stretched by the motion of the linear stage. Over the course of the deformation, the resulting force is constantly recorded with a frequency of 10 data points per second. The force transducer (precision limit of ±0.01 g) is connected to a PC with a custom-made LabView system.

In order to conduct various experiments under thermo–electro–mechanical loads, the testing equipment was modified as depicted in Fig. 4. Compared to the initial setup of the custom testing device, the height of the safety cabinet (**7**) had to be increased in order to enable a sufficient range of displacement inside the added thermo chamber. Furthermore, at the rear of the cabinet, a heating system (**8**) was installed that can be connected to a compressed air supply.

The heating system contains a heating element that increases the temperature of the air flow, which is directed into the thermo chamber (**9**) through the flexible tube (**10**). Both the thermo chamber and the heating system are produced from temperature resistant Teflon that can withstand high temperatures and is not electrically conductive, so that experiments with high voltages can be performed. The additional thermal chamber is fixed at the base of the safety cabinet and contains a mounting for the clamping plates (**2**) at the internal bottom surface. Thus, when compared to the earlier experimental setup, the stretch direction is reversed, i.e. the sample (**1**) is now fixed at the bottom and deformed by the linear stage (**3**) in upwards direction. In order to allow for a sufficiently large displacement of the sample within the added thermo chamber, the top pair of clamping plates is connected to the linear stage via a 300 mm long rod that is placed through a drilling at the top of the thermo chamber and is connected to the linear stage via the force transducer (**4**). Both the rod and the clamping plates are produced from PEEK (polyether ether ketone) material that provides the necessary heat resistance and mechanical stiffness without being electrically conductive. The frame of the testing system (**5**) remained unchanged compared to the initial setup. In addition to the modifications necessary for the temperature regulation, the cable management was modified significantly in order to increase work safety. The bottom clamps are therefore designed with a metallic connector for the electric wiring that is directly attached to the sample. As the material is stretched upwards and the bottom clamps are fixed, the wiring (**6**) does not move during the deformation of the material, effectively eliminating the need for a flexible connection of the cable via a strip of aluminum foil. The heating system is controlled by an external control unit (**11**) that is connected to the laboratory PC. In the right part of Fig. 4, the high voltage power supply (**12**) is visible, placed on top of the thermal control unit.

The data obtained by the conducted experiments is presented in the following sections by plotting the resulting force over the applied stretch, as the force is directly measured by the load cell during the tests. This comes with the downside that the results of the experiments conducted with different sized cross sections cannot be directly compared, as the resulting force depends on the cross sectional area. In the case of the mechanical and thermo–mechanical tests this could potentially be solved by transferring the measured force to an appropriate stress measure, as it is assumed that, due to the selected dimensions of the samples, the deformation state and the resulting stress in the middle of the specimen is constant. However, in the experiments involving an electric field, the dimensions of the material sample do not allow for a conversion of the measured force to a single stress quantity, as the stress distribution cannot be considered to be constant. Thus, for the sake of consistency, we choose to keep the selected format of plotting the resulting force over the applied stretch.

3. Experiments on VHB 4905™

In this section the results of the experiments conducted on the widely used dielectric elastomer VHB 4905™ produced by 3M™ are presented. This commercially available, double sided bonding tape with a thickness of 500 μm is used frequently in the context of electro-active polymers, especially in the design of laboratory-originated prototypes, due to its high stretchability and moderate dielectric properties. However, the interested reader should note that the sticky surface in combination with the considerably soft behavior makes VHB quite challenging to handle during the experiments, especially when additional sample preparation is required. The aim of these experiments is to acquire a full set of thermo–electro–mechanical data that is well suited for a subsequent identification of a set of material parameters appearing in a continuum-based thermo–electro–viscoelastic constitutive model at finite strains (that will be presented in the second part of this contribution). In order to distinguish between the mechanical response of the material and the influence of a thermal or electric field, the experiments are conducted step-by-step, beginning with purely mechanical tests performed at room temperature, i.e. reference temperature $\Theta_0 = 23$ °C. Subsequently, the results of similar experiments at increased temperatures are presented, followed by the results of tests performed under the application of an electric field. Finally, we show the results of the combination of thermo–electric loading with a mechanical deformation. It should be noted that in all of these experiments special care is taken so that the material is not deformed significantly prior to the actual experiment. Especially in the case of electro–mechanical experiments, the results published in the literature are frequently obtained with samples that are prestretched in order to amplify the effect of the electric field, c.f. Hossain et al. (2015). However, this prestretch creates a more complex loading scenario that has to be measured and evaluated correctly in order to allow for an intended identification of the electro-mechanical coupling material parameters.

Unless stated otherwise, for each of the presented tests at least eight separate experiments are performed for each loading condition in order to assure reproducibility. For each of these individual experiments a fresh test sample cut from one roll of VHB 4905™ is used. Such a consistent sample selection reduces the influence of possible material imperfections. For the sake of readability, error estimations, such as the standard deviation of the collective experiments, are not depicted in the plots but only mentioned in the respective description. Furthermore it should be noted that experiments were carried out to investigate the influence of the so-called Mullins effect, i.e. a permanent softening of the material after the first deformation. However, no such effect was observed and therefore, Mullins effect tests are not included in the following sections.

3.1. Mechanical experiments

For the mechanical experiments, material samples with the dimensions 130 mm by 10 mm are cut from a 60 m roll of VHB 4905™ with the width of 300 mm. The test samples are mounted into the *Inspekt 5 kN* so that the distance between the clamps is exactly 100 mm. No further sample preparation is required for the purely mechanical experiments. As it is well documented that VHB shows a highly viscoelastic material response (Hossain et al., 2012, 2015; Mehnert and Steinmann, 2019; Mehnert et al., 2019), multi-step relaxation tests and cyclic loading–unloading tests are conducted. It can be assumed that the viscous stress contributions
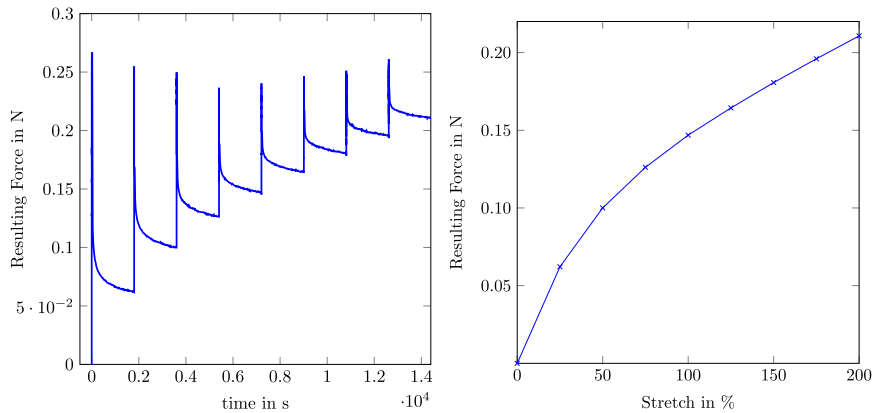
Fig. 5. (Left) Loading procedure during a multi-step relaxation test over time and (right) resulting force of a multi-step relaxation test at constant reference temperature.

vanish over time, when the deformation applied to the sample is kept constant. Consequently, the remaining stress can be associated with the elastic response of the material. In order to identify these elastic responses at different deformations, multi-step relaxation tests as presented in Fig. 5 are performed.

The plot on the left-hand side of Fig. 5 shows the procedure of a multi-step relaxation test. Over the course of eight consecutive steps, the applied strain on the test sample is increased. In every step, a deformation of 25% is applied at the maximum displacement velocity of the tensile test machine, i.e. 33 mm/s. This rapid deformation results in an initial peak of the resulting force. Subsequently, the sample is held in the deformed state for thirty minutes, which is the relaxation time considered in Hossain et al. (2012). It is assumed that after this period the material has reached a state close to the equilibrium. It should be noted that significantly longer holding periods would lead to a closer approximation of a configuration in which the polymer chains on the microscale are completely relaxed. However, such a holding period is not feasible for the multistep relaxation experiments presented here, especially with the aim of ensuring reproducibility by performing the tests multiple times. Furthermore, it is assumed that for a wide range of applications the high deformation rates lead to a clear dominating role of the viscous material response. Therefore, a holding period of thirty minutes is considered as sufficient in the scope of this work. More experiments were also conducted taking sixty minutes as the holding time. However, no further significant change in the resulting force was recorded. Over the course of this relaxation period, the resulting force converges asymptotically towards a time-independent equilibrium state, where we can assume that the resulting force originates from the elastic stress contributions only. The difference between the total stress and the equilibrium stress is known as the overstress, which is characteristic for the viscous part of the material response (Haupt, 2013). Following the relaxation period, another deformation of 25% is applied with a subsequent relaxation time until the maximum deformation of 200% is reached. When we plot the equilibrium force over the applied strain the equilibrium curve is obtained as depicted in the right plot of Fig. 5. The increase of the equilibrium force over the applied strain is clearly visible. However, it only shows the strain softening phase of the material response. The subsequent strain hardening behavior resulting in the classical S-shape curve of the equilibrium stress–strain response, which is the characteristic of many polymeric materials, is not visible. In the case of VHB, this shape is only identifiable for significantly higher applied strains. For instance, Liao et al. (2020) performed multi-step relaxation tests on VHB 4910 with a maximum applied strain of 800% in which the material clearly demonstrated the S-shape curve of rubber elasticity. In the context of the current work, we restrict ourselves to a deformation of 200% for several reasons. First, strains higher than 200% are not practical in the case of a combined thermo–electro–mechanical loading condition. For instance, most of the actuator devices used in soft robotics, stretch sensors in wearable devices and energy harvesters made of DEs operate within the range of 100% strain (Amjadi et al., 2012; Collins et al., 2021). Second, our ultimate intention is to investigate the material under combined loading scenarios and to produce enough experimental data for feeding a finite strain thermo–electro–viscoelastic constitutive model. Third, 200% strain is selected partly due to dimensional constraints of the testing equipment and partly due to the electric breakdown of the material. The calculated relative standard deviation between the individual experiments does not exceed 3% in any of the steps, showing a good reproducibility of the experiments.

Following the characterization of the elastic behavior of the material by multi-step relaxation tests, the results of cyclic loading tests with various strain velocities are evaluated in order to obtain information on the viscous material response. In these experiments, the sample is stretched at a constant deformation rate to a maximum stretch of 200%. Once this value is reached, the strain is instantly decreased until the testing device has returned to its initial position. As stated before, the experiments are repeated multiple times with the aim of reducing the influence of undesired factors, such as material imperfections or deviations in the width of the manually cut samples. In order to give the reader an impression on the variance in the experiments, the curves of all ten individual cyclic loading tests at the strain rate of 0.2 s^{-1} are presented in Fig. 6 as thin solid lines. Additionally, the resulting average curve that will subsequently be used in the calculations, is added as thick black line.

The mean value of the calculated relative standard deviation of these ten experiments is well below 6% and therefore verifies a good reproducibility of all the experiments. In order to fully characterize the viscoelastic material response of the VHB polymer, it
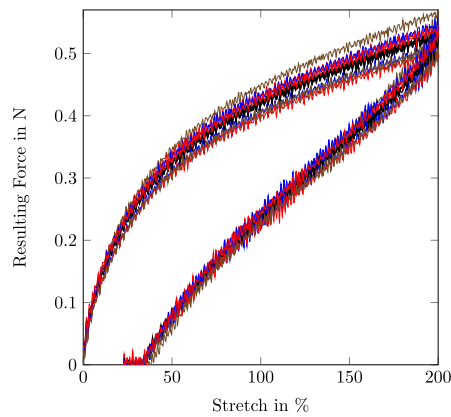
Fig. 6. Resulting force over the applied stretch of ten individual cyclic loading tests at a strain rate of 0.2 s^{-1} performed at room temperature. Thick black curve shows the resulting average force.
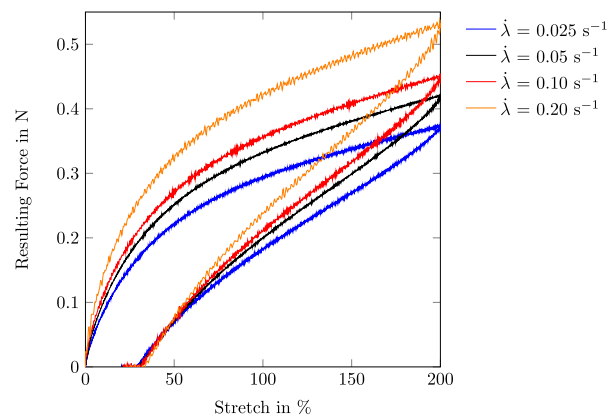

Fig. 7. Averaged resulting force over the applied stretch of cyclic loading tests at different strain rates performed at room temperature.

is necessary to conduct cyclic loading experiments over a wide range of different strain rates. A comparison of the averaged results of all tested strain rates is depicted in Fig. 7. In all of the following Figures, the plotted results show an average of a number of ten experiments unless stated otherwise.

The response of the material clearly shows a hysteresis curve that originates from a time dependent viscoelastic material behavior. It should be noted as well that the size of the hysteresis depends directly on the strain rate, i.e. the area encircled by a loading curve and the corresponding unloading curve increases with the increase in the deformation rate. Furthermore, Fig. 7 shows an increase in the resulting force for faster deformations. This behavior is expected as the influence of the viscous stress component increases at higher deformation rates. In summary, the purely mechanical material response of VHB 4905™ can be characterized as viscoelastic with a rate dependency that is already significantly pronounced for strain rates between 0.025 s^{-1} and 0.2 s^{-1}. It should be noted that the experiments are restricted to only one deformation cycle due to the special material behavior of VHB. The highly viscous material response in combination with the double sided bonding surface frequently results in an adhering of the material to itself or the testing equipment, when the sample is folding in the unloading phase during the experiments. These scenarios render the tests useless for the material characterization.

3.2. Thermo–mechanical experiments

In the previous section, the behavior of VHB polymer was investigated at room temperature of 23 °C by relaxation experiments to characterize the purely elastic response and by cyclic loading tests at various strain rates for the investigation of its viscous behavior. Now the same sets of experiments are performed at elevated thermal conditions in order to demonstrate the influences of temperature on the material response, particularly on its stress–strain responses. Thus, prior to any test, temperature inside the thermal chamber is set to the desired value and then the material sample is mounted. Due to the small thickness of a sample (0.5 mm), a heat-up time of 10 min before the conduction of any experiments has proven to be sufficient for the sample to induce with the temperature of the chamber. After the heating time, multi-step and cyclic loading tests are performed, which are identical to the experiments conducted in the previous section at reference temperature. Thanks to our previous experience on the thermo–viscoelastic experiments for VHB
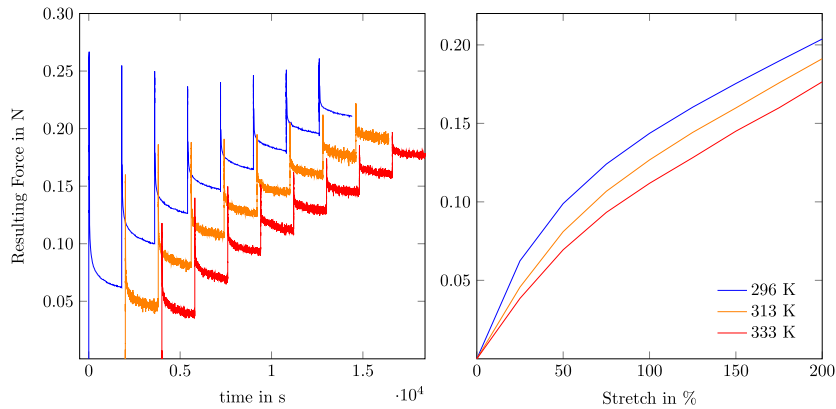
Fig. 8. (Left) Resulting force over time and (right) resulting equilibrium values of the resulting force of a multi-step relaxation test at different temperatures.

4910, c.f. Liao et al. (2020), in an effort to observe the influences of temperature, a temperature interval is selected ranging from room temperature to a maximum value of 60 °C. The maximum temperature is selected under the assumption that electro-active polymers used neither in actuators (e.g., artificial muscles), sensors (e.g., wearable devices) nor energy harvesters will experience temperature higher than this limit. However, a further decrease below room temperature is considered as a necessary addition to the obtained thermo–mechanical data set, which was impossible due to the capabilities of the available equipment during the experimental investigations. The first temperature increase is to 30 °C while the remaining range is tested in steps of 10 °C. Fig. 8 shows the results of the multi-step relaxation tests performed at various thermal conditions. For the sake of better illustration, only the results at 40 °C and 60 °C in combination with the results at the reference temperature are depicted. In the left plot, the force over the entirety of the experiment is depicted. The data of each individual temperature is plotted with an offset on the time axis, in order to further enhance their visualization. The plot on the right-hand side shows the equilibrium curves.

It is clearly visible that even comparably small temperature changes lead to a noticeable change in the elastic response of the VHB samples. As the temperature is increased, the resulting force decreases over the entire course of the experiment, which is depicted in the left plot of Fig. 8. Consequently, the values of the equilibrium curves shown in the right plot of Fig. 8 decrease as well. It should be noted that the noise in the depicted results, visible especially during the relaxation periods in the left plot of Fig. 8, is more pronounced for the experiments, in which the temperature of the samples is increased. This is due to the air flow inside the thermal chamber that is used for the temperature regulation, which leads to a vibration of the mounted sample.

In order to characterize the influence of a temperature increase on the material, Fig. 9 shows the resulting force at the maximum applied deformation of 200% over the temperature range of all tested temperatures. The solid trend line that is added in order to indicate the general behavior, shows a slightly nonlinear response of the material to the change in temperature. However, it has to be emphasized that this simple relation between the temperature and the mechanical response is only valid for the small temperature range considered in the scope of this work. Especially, when the temperature approaches the glass transition range of the material, the effects of the temperature are highly nonlinear as presented for example in the works of Sheng et al. (2012b) and Srivastava et al. (2010).

Next, the effect of the temperature on the viscous properties of the material are investigated. To this end, cyclic loading tests at different strain rates are performed. For each strain rate, the temperature inside the thermal chamber is varied in steps of 10 °C up to a maximum value of 60 °C. The effect of the temperature is equivalent to the one visible during the multi-step relaxation tests, as depicted in Figs. 10–13. In each of the figures, the plot on the left-hand side shows the material response during a cyclic loading test at the temperatures 23 °C, 40 °C and 60 °C over the entire deformation range. The plot on the right-hand side of each figure presents the resulting force at the maximum applied stretch of 200% for all of the selected temperatures with a trend line, indicating the general behavior.

All relevant results show significant thermal sensitivity of the material, which is independent of the applied strain rate. In this case, an increase in temperature leads to a softening of the material resulting in a decrease in the total force. Furthermore, the figures imply a decrease in the area of the hysteresis loop as an additional effect of the temperature on the viscous characteristics of the material. It is apparent that the trend line in Fig. 12 shows a different curvature compared to the other strain rates. However, due to the narrow temperature range selected in this study for the experiments, this difference is not attributed to an alternate material behavior but deviations during the conducted experiments. As a first quantification of the thermal influence, we can calculate the ratio between the resulting force at the maximum applied stretch at room temperature and the respective value at 60 °C. While for the slowest strain rate of 0.025 s^{-1}, this ratio is approximately 0.75, the ratio decreases with increasing strain rates to 0.67 at the strain rate of 0.2 s^{-1}, indicating that the influence of the temperature on the viscous material response is reduced for an increase of the deformation rate. It should be noted however that it is not possible to directly analyze the magnitude of the effect of the temperature on the viscous nature of the material exclusively from the results of the cyclic loading tests shown in Figs. 10–13, as the plotted curves inevitably show a combination of both the elastic and the viscous response.
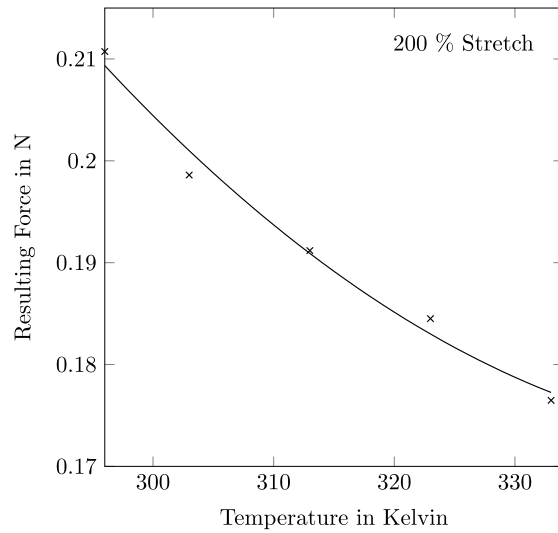
Fig. 9. Resulting equilibrium values of the force at the maximum applied stretch of 200% during multi-step relaxation tests conducted at various temperatures.
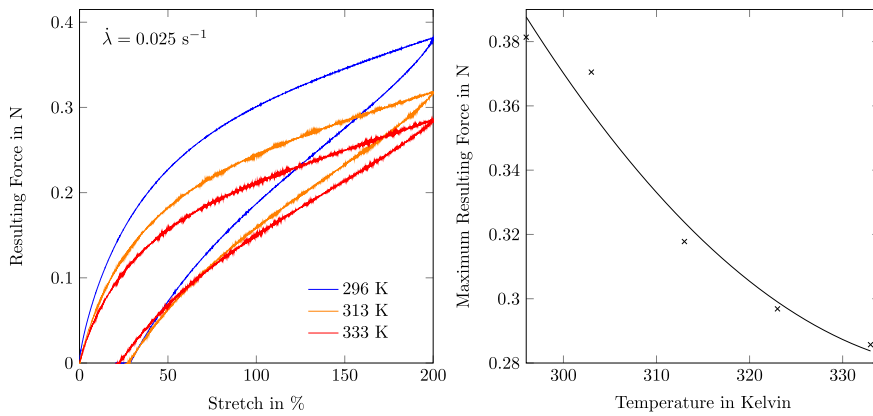

Fig. 10. Resulting force of cyclic loading tests at various temperatures at a strain rate of $\dot{\lambda} = 0.025$ s^{-1} (left) over the entire stretch, (right) for the maximum applied stretch over the entire temperature range.

Fig. 11. Resulting force of cyclic loading tests at various temperatures at a strain rate of $\dot{\lambda} = 0.05$ s^{-1} (left) over the entire stretch, (right) for the maximum applied stretch over the entire temperature range.
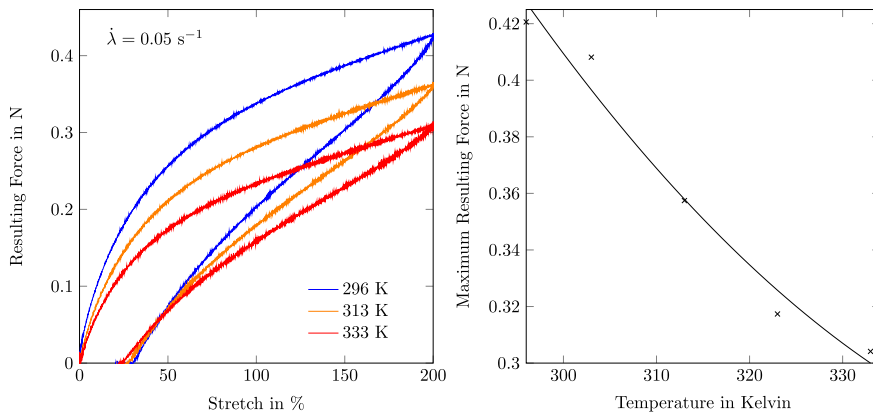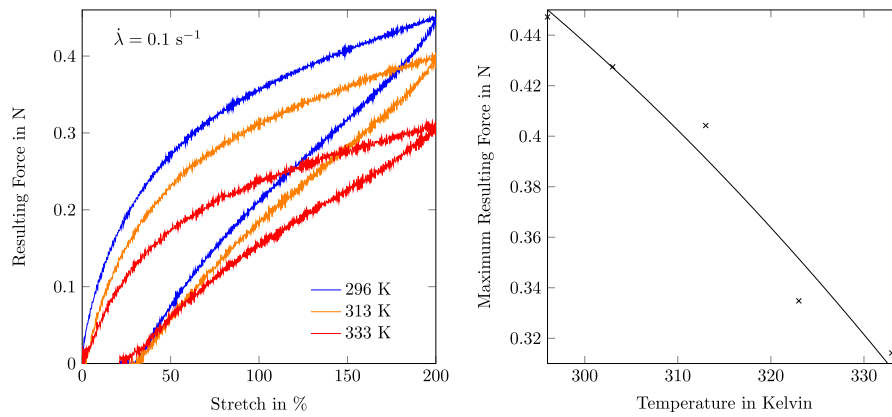
Fig. 12. Resulting force of cyclic loading tests at various temperatures at a strain rate of $\dot{\lambda} = 0.1\ \text{s}^{-1}$ (left) over the entire stretch, (right) for the maximum applied stretch over the entire temperature range.

Fig. 13. Resulting force of cyclic loading tests at various temperatures at a strain rate of $\dot{\lambda} = 0.2\ \text{s}^{-1}$ (left) over the entire stretch, (right) for the maximum applied stretch over the entire temperature range.
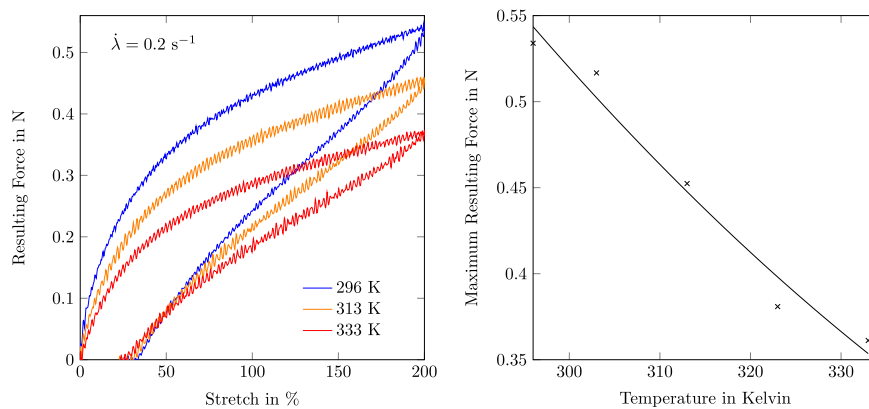
3.3. Electro-mechanical experiments

In this section, we present combined electro–mechanical experiments on VHB 4905™ for the sake of completeness even though the results are the same as published in Mehnert et al. (2019). As mentioned earlier, the experiments that include the application of an electric field could not be conducted with the same test-setup as the thermo–mechanical experiments, as the *Inspekt 5 kN* is not equipped for the application of an electric field on the test sample during the experiments, i.e. a high-voltage power source, appropriate cable management and work safety precautions. As the experiments require a significant amount of preparation and are frequently prone to electric breakdown due to defects of the material or inaccuracies during the preparation process, the number of experiments, over which the presented results are averaged, is only five.

In contrast to the experiments presented in the previous sections, the sample width in this section has to be increased. Such an increment in the width of the sample provides additional spaces for the application of the electric field. Moreover, additional preparations are required for conducting the electro-mechanical tests. The material samples have a width of 100 mm, which is necessary for the application of an electrically conductive coating on both sides of the material that acts as compliant electrodes. In order to prevent any electric short circuiting, an area at the edges of the sample has to remain uncoated, while simultaneously the ratio between the coated and uncoated area has to be maximized to amplify the effect of the electric field. In a first step of the sample preparation, one of the top and one of the bottom clamping plates are placed onto a holding frame, which fixes the distance between the plates at 70 mm. Next, the VHB sample is placed on the clamping plates, thus the length of the material that is deformed during the experiments is exactly 70 mm. Subsequently, the protective covering of the VHB tape is removed and the remaining pair of plates are put on the top of the sample. The top and bottom plate pairs are each fixed by a pair of screws, which, in combination with the bonding properties of VHB 4905™, is sufficient to prevent the material sample from slipping out of the fixation during the deformation process. Now, the top side of the sample is covered with conductive carbon grease using a soft brush. A small stripe on each side and over the entire length of the edge has to remain uncoated, in order to prevent short circuiting once the electric voltage is applied. For this, an area with the width of approximately 5 mm is covered with pieces of the previously removed protective covering, which simplifies the application of the carbon grease (left picture of Fig. 14).
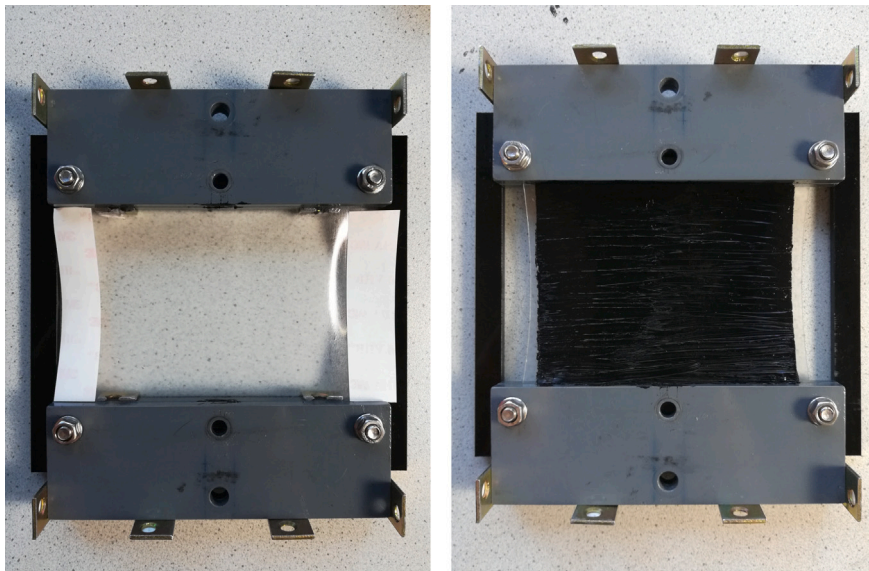
Fig. 14. Specimen of VHB 4905™ (left) with protective covering before and (right) after the application of the conductive coating.
Source: Figure taken from Mehnert et al. (2019).

Once the face of the sample is painted, the protective covering is removed, which results in a precise boundary of the coated area. As long as only one side of the VHB sample is coated, it can easily be ensured that the surface is continuously covered by a visual examination. In order to paint the backside of the material with carbon grease as well, the holding frame with the sample is flipped. Due to the transparency of the VHB tape, the uncovered area at the edges of the front side is visible, which can be used as a boundary when the backside is painted (right picture in Fig. 14). After both sides are coated, a flexible connection of the grease coating with the stiff electric wires has to be established. For this, a stripe of aluminum foil is glued to the bottom holding clamps, so that one end of the stripe slightly touches the grease coating and the other end of the foil is free to move. Eventually, the prepared sample is mounted inside the testing device and the frame is removed carefully to ensure that the material is not put under an unintentional prestretch. In a final step, a second stripe of aluminum foil is fixed to the other side of the sample, in order to connect the second electric wire. With the prepared samples, cyclic loading tests are performed under the application of an electric field in thickness direction. The tests were performed at strain velocities of 0.025 s^{-1}, 0.1 s^{-1} and 0.2 s^{-1}. A constant potential difference between the compliant electrodes is applied over the entire course of the deformation. It can be assumed to be supplied instantaneously once the power source is activated. Before the mechanical deformation of the sample is initiated the sample is held under the purely electric loading for one minute. As the influence of the electric field becomes visible only at sufficiently high field strengths, voltages of 2 kV, 3 kV, 4 kV, 5 kV and 6 kV are applied. Experiments with voltages above 6 kV could not be performed successfully due to electric breakdown of the material. As reference, tests in the absence of an electric field are performed. The results of these experiments are depicted in Figs. 15–17.

On the left-hand side, the results over the entire loading cycle of 200% are depicted. This includes the purely mechanical case (dark blue solid line) as a reference and the results for a potential difference of 4 kV (green solid line) and 6 kV (light blue solid line). On the right-hand side the value of the force at the maximum applied strain of 200% is shown for all applied voltages. Here, a solid line is included in order to indicate a general trend of the effect of the electric field. The curves plotted in Figs. 15–17 represent averaged values of five experiments, each one performed with an individual material sample. The mean standard deviations between these individual tests are below 5% for all the tested velocities and over the entire test cycle. Thus, the tests show a good reproducibility. The influence of the applied electric field on the material response becomes clearly visible in the results. For all applied deformation velocities the resulting forces are reduced, due to the applied electric field and the effect increases with an increased deformation of the sample. When we focus on the resulting force at the maximum value of deformation, the decline due to the electric field is approximately 7% for a strain rate of 0.2 s^{-1} and approximately 9% for 0.1 s^{-1} and 0.025 s^{-1}. Furthermore, the depicted trend line indicates a nonlinear effect of the electric field on the material response. It should be noted that the application of the electric field prior to the mechanical deformation leads to an expansion of the material sample. Therefore the graphs of the experiments with an applied electric field do not start exactly at a resulting force of 0 N but slightly below the x-axis.

3.4. Thermo–electro–mechanical experiments

Finally, experimental results of VHB 4905™ polymer with a combination of all three loading types, i.e., mechanical, thermal and electric, are presented in the following section. In order to perform thermo–electro–mechanical experiments, material samples with the same dimensions as for the electro-mechanical tests at reference temperature are cut and coated with carbon conductive grease.
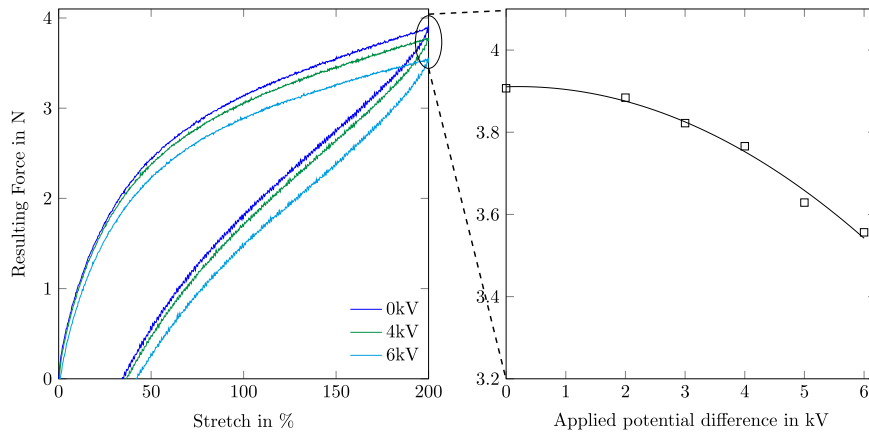
Fig. 15. Loading–unloading test for a strain rate of $\dot{\lambda} = 0.025$ s^{-1}. (Left) Resulting force over the entire loading–unloading cycle. (Right) Resulting force at the maximum strain value for all applied potential differences.
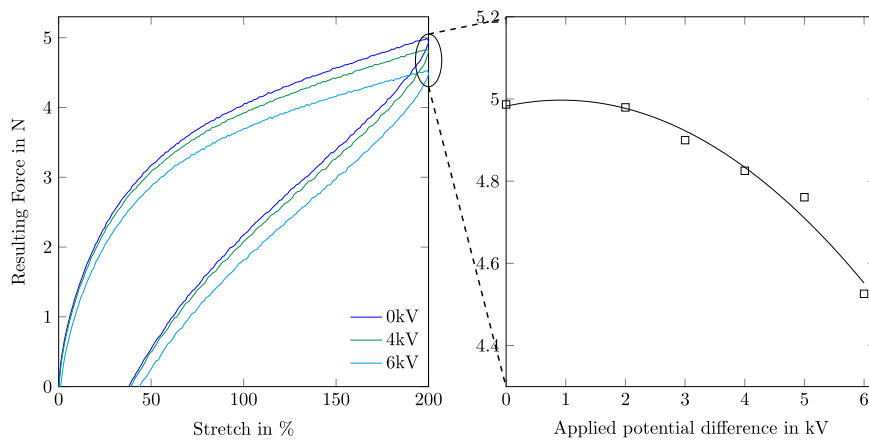*Source:* Figure taken from Mehnert et al. (2019).

Fig. 16. Loading–unloading test for a strain rate of $\dot{\lambda} = 0.1$ s^{-1}. (Left) Resulting force over the entire loading–unloading cycle. (Right) Resulting force at the maximum strain value for all applied potential differences.
Source: Figure taken from Mehnert et al. (2019).

Fig. 17. Loading–unloading test for a stretch rate of $\dot{\lambda} = 0.2$ s^{-1}. (Left) Resulting force over the entire loading–unloading cycle. (Right) Resulting force at the maximum strain value for all applied potential differences.
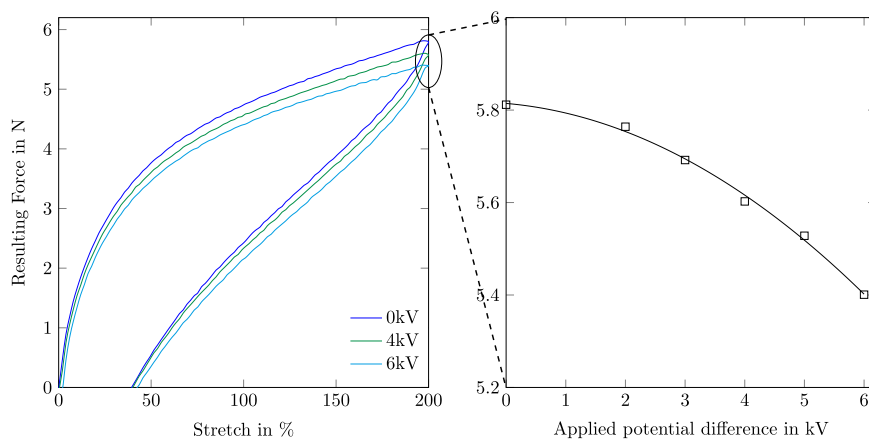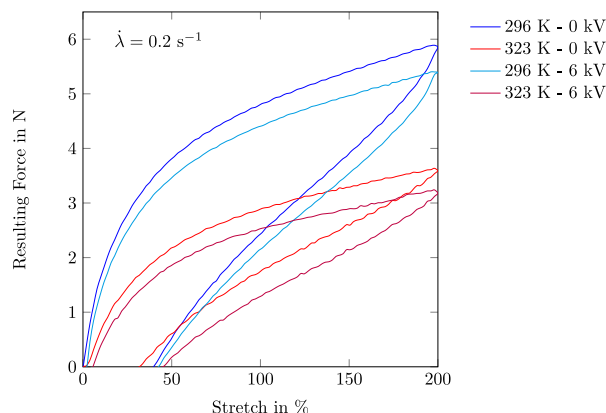*Source:* Figure taken from Mehnert et al. (2019).

Fig. 18. Resulting force over the applied stretch of cyclic loading tests at different temperatures and applied electric voltages.

After the prepared sample is mounted onto the machine, the thermo chamber is closed and the target temperature is set. Once the thermo chamber is heated, the material is given fifteen minutes to fully heat up. After this wait time, the cyclic loading tests are conducted. Fig. 18 presents a comparison between a purely mechanical, electro-mechanical, thermo–mechanical and thermo–electro–mechanical cyclic loading test. Due to the further increased complexity of thermo–electro–mechanical experiments, we confine ourselves to conduct experiments at the temperature of 50 °C with a strain rate of 0.2 s^{-1}.

As can be expected, the combination of the electrical and thermal loading results in a superposition of the individual effects. It is clearly visible that the temperature change has a significantly more pronounced effect on the material response than the electric field even at the moderate change of a few tens of Kelvin. When concentrating on the force resulting from the maximum deformation of 200%, it can be seen that the relative decrease of the force due to the applied electric field is around 10%, both for the experiments conducted at room temperature and at 50 °C. Thus, from the experiments under consideration, it can be assumed that no additional coupling between the thermal and the electric loading takes place. In the initial stages of the deformation at 323 K (red curve) the depicted graph shows a slightly 'J-shaped' curve which has to be attributed to minor imperfections of the mounting position of the sample that settle in after the heating time.

4. Summary and outlook

In this contribution, we present a comprehensive thermo–electro–viscoelastic experimental study on one of the classical polymers widely used as an electro-active polymer, i.e., VHB 4905™. The behavior was investigated using multistep relaxation tests for the characterization of the elastic material properties and cyclic loading–unloading experiments for the viscous responses. These tests were performed at room temperature to establish an underlying purely mechanical behavior and at increased temperatures to investigate the influence of temperature change. For the sake of completeness, the results of a set of electro-mechanical experiments were presented, in which cyclic loading tests with three different strain rates and an electric potential difference applied normal to the stretch direction were performed. Finally, the results of experimental studies with a combination of all three types of loading were presented. During these experiments, the influence of a temperature increase and the electric field becomes clearly visible. It is intended to use the experimental results presented herein for the validation of a thermo–electro–viscoelastic constitutive model that will be summarized in Part II of the contribution. In the future, similar characterizations will also be performed for different materials such as silicones filled with piezoactive particles that amplify the electro-mechanical coupling. Furthermore, the investigation of the influence of the temperature on the electromechanical instability behavior of the material will be investigated both numerically, based on the identified material parameters, and experimentally as a validation of the theoretical approach.

Declaration of competing interest

The authors declare that they have no known competing financial interests or personal relationships that could have appeared to influence the work reported in this paper.

Acknowledgments

References

Amjadi, M., Pichitpajongkit, A., Lee, S., Ryu, S., I., P., 2012. Highly stretchable and sensitive strain sensor based on silver nanowire-elastomer nanocomposite. ACS Nano 8, 5154–5163.

Bar-Cohen, Y., 2002. Electroactive polymers: current capabilities and challenges. In: SPIE's 9th Annual International Symposium on Smart Structures and Materials. International Society for Optics and Photonics, pp. 1–7.

Bar-Cohen, Y., 2004. Electroactive Polymer (EAP) Actuators As Artificial Muscles: Reality, Potential, and Challenges, Vol. 136. SPIE Press.

Bhagawan, S., De, S.K., 1988. Mechanical properties and fracture surface morphology of clay-filled thermoplastic 1, 2-polybutadiene rubber at elevated temperatures. Polym.-Plast. Technol. Eng. 27 (1), 37–60.

Böse, H., Fuß, E., 2014. Novel dielectric elastomer sensors for compression load detection. In: SPIE Smart Structures and Materials+ Nondestructive Evaluation and Health Monitoring. International Society for Optics and Photonics, p. 905614.

Bustamante, R., 2009. Transversely isotropic non-linear electro-active elastomers. Acta Mech. 206 (3–4), 237.

Carpi, F., Anderson, I., Bauer, S., Frediani, G., Gallone, G., Gei, M., Graaf, C., Jean-Mistral, C., Kaal, W., Kofod, G., et al., 2015. Standards for dielectric elastomer transducers. Smart Mater. Struct. 24 (10), 105025.

Collins, I., Hossain, M., Dietmer, W., Masters, I., 2021. Flexible membrane structures for wave energy harvesting: A review of the developments, materials and computational modelling approaches. Renew. Sustain. Energy Rev. 151, 111478.

Diaconu, I., Dorohoi, D.-O., Ciobanu, C., 2006. Electromechanical response of polyurethane films with different thickness. Rom. J. Phys. 53 (1–2), 91–97.

Dorfmann, A., Ogden, R., 2005. Nonlinear electroelasticity. Acta Mech. 174 (3–4), 167–183.

Ferry, J.D., 1980. Viscoelastic Properties of Polymers. John Wiley & Sons.

Guo, Y., Liu, L., Leng, J., 2021. Thermo-electromechanical instability of dielectric elastomer undergoes polarization saturation and temperature variation. Acta Mech. Sinica 37 (3), 414–421.

Guo, J., Xiao, R., Park, H.S., Nguyen, T.D., 2015. The temperature-dependent viscoelastic behavior of dielectric elastomers. J. Appl. Mech. 82 (9), 091009.

Ha, S.M., Yuan, W., Pei, Q., Pelrine, R., Stanford, S., 2006. Interpenetrating polymer networks for high-performance electro-elastomer artificial muscles. Adv. Mater. 18 (7), 887–891.

Haupt, P., 2013. Continuum Mechanics and Theory of Materials. Springer Science & Business Media.

Hossain, M., Vu, D.K., Steinmann, P., 2012. Experimental study and numerical modelling of VHB 4910 polymer. Comput. Mater. Sci. 59, 65–74.

Hossain, M., Vu, D.K., Steinmann, P., 2015. A comprehensive characterization of the electro-mechanically coupled properties of VHB 4910 polymer. Arch. Appl. Mech. 85 (4), 523–537.

Koh, S.J.A., Keplinger, C., Li, T., Bauer, S., Suo, Z., 2011a. Dielectric elastomer generators: How much energy can be converted? IEEE/ASME Trans. Mechatronics 16 (1), 33–41.

Koh, S.J.A., Li, T., Zhou, J., Zhao, X., Hong, W., Zhu, J., Suo, Z., 2011b. Influence of the temperature and deformation-dependent dielectric constant on the stability of dielectric elastomers. J. Polym. Sci. B: Polym. Phys. 49 (7), 504–515.

Li, B., Chen, H., Zhou, J., Zhu, J., Wang, Y., 2011. Polarization-modified instability and actuation transition of deformable dielectric. EPL(EuroPhys. Lett.) 95 (3), 37006.

Liao, Z., Hossain, M., Yao, X., Mehnert, M., Steinmann, P., 2020. On thermo-viscoelastic experimental characterization and numerical modelling of VHB polymer. Int. J. Non-Linear Mech. 118, 103263.

Lion, A., 1997a. On the large deformation behaviour of reinforced rubber at different temperatures. J. Mech. Phys. Solids 45 (11), 1805–1834.

Lion, A., 1997b. A physically based method to represent the thermo-mechanical behaviour of elastomers. Acta Mech. 123 (1–4), 1–25.

Lion, A., 2000. Thermomechanik Von Elastomeren. Institut für Mechanik, Universität Kassel.

Liu, L., Liu, Y., Li, B., Yang, K., Li, T., Leng, J., 2011. Thermo-electro-mechanical instability of dielectric elastomers. Smart Mater. Struct. 20 (7), 075004.

Mehnert, M., Hossain, M., Steinmann, P., 2019. Experimental and numerical investigations of the electro-viscoelastic behavior of VHB 4905TM. Eur. J. Mech. A Solids 77, 103797.

Mehnert, M., Steinmann, P., 2019. On the influence of the compliant electrodes on the mechanical behavior of VHB4905. Comput. Mater. Sci. 160, 287–294.

O'Halloran, A., O'Malley, F., McHugh, P., 2008. A review on dielectric elastomer actuators, technology, applications, and challenges. J. Appl. Phys. 104 (7), 9.

Pelrine, R., Kornbluh, R., Kofod, G., 2000a. High-strain actuator materials based on dielectric elastomers. Adv. Mater. 12 (16), 1223–1225.

Pelrine, R., Kornbluh, R., Pei, Q., Joseph, J., 2000b. High-speed electrically actuated elastomers with strain greater than 100%. Science 287 (5454), 836–839.

Sheng, J., Chen, H., Li, B., 2011. Effect of temperature on the. stability of dielectric elastomers. J. Phys. D : Appl. Phys. 44 (36), 365406.

Sheng, J., Chen, H., Li, B., Wang, Y., 2013. Influence of the temperature and deformation-dependent dielectric constant on the stability of dielectric elastomers. J. Appl. Polym. Sci. 128 (4), 2402–2407.

Sheng, J., Chen, H., Li, B., Wang, Y., Qiang, J., 2012a. Effect of temperature on electromechanical instability of dielectric elastomers. Electroact. Polym. Actuators and Devices (EAPAD) 8340, 83403B.

Sheng, J., Chen, H., Qiang, J., Li, B., Wang, Y., 2012b. Thermal, mechanical, and dielectric properties of a dielectric elastomer for actuator applications. J. Macromol. Sci. Part B 51 (10), 2093–2104.

Srivastava, V., Chester, S.A., Ames, N.M., Anand, L., 2010. A thermo-mechanically-coupled large-deformation theory for amorphous polymers in a temperature range which spans their glass transition. Int. J. Plast. 26 (8), 1138–1182.

Treloar, L.R.G., 1975. The Physics of Rubber Elasticity. Oxford University Press, USA.

Vertechy, R., Fontana, M., Papini, G.R., Forehand, D., 2014. In-tank tests of a dielectric elastomer generator for wave energy harvesting. In: SPIE Smart Structures and Materials+ Nondestructive Evaluation and Health Monitoring. International Society for Optics and Photonics, p. 90561G.

Wang, S., Decker, M., Henann, D.L., Chester, S.A., 2016. Modeling of dielectric viscoelastomers with application to electromechanical instabilities. J. Mech. Phys. Solids 95, 213–229.

Zhang, J., Sheng, J., Liu, X., Liu, L., Zhao, J., Chen, H., 2020. Temperature effect on electromechanical properties of polyacrylic dielectric elastomer: An experimental study. Smart Mater. Struct. 29 (4), 047002.